High-spin states in ^{191,193}Au and ^{192}Pt: Evidence for oblate deformation and triaxial shapes

Y. Oktem,[1] D. L. Balabanski,[2] B. Akkus,[1] C. W. Beausang,[3,4] M. Bostan,[1] R. B. Cakirli,[1] R. F. Casten,[3] M. Danchev,[5] M. Djongolov,[5] M. N. Erduran,[1] S. Erturk,[6] K. A. Gladniski,[7] G. Gürdal,[8] J. Tm. Goon,[9] D. J. Hartley,[5,10] A. A. Hecht,[3,11] R. Krücken,[3] N. Nikolov,[5,7] J. R. Novak,[3] G. Rainovski,[7] L. L. Riedinger,[5] I. Yigitoglu,[12] N. V. Zamfir,[3,13] and O. Zeidan[5]

[1]*Department of Physics, Istanbul University, Vezneciler, 34459 Istanbul, Turkey*
[2]*Institute for Nuclear Research and Nuclear Energy, Bulgarian Academy of Sciences, BG-1784 Sofia, Bulgaria*
[3]*Wright Nuclear Structure Laboratory, Yale University, New Haven, Connecticut 06520, USA*
[4]*Department of Physics, University of Richmond, Richmond, Virginia 23173, USA*
[5]*Department of Physics and Astronomy, University of Tennessee, Knoxville, Tennessee 37996, USA*
[6]*Department of Physics, Nigde University, 51200 Nigde, Turkey*
[7]*Faculty of Physics, St. Kliment Ohridski University of Sofia, BG-1164 Sofia, Bulgaria*
[8]*Clark University, Worchester, Massachusetts 01610, USA*
[9]*Department of Physics and Astronomy, Louisiana State University, Baton Rouge, Louisiana 70803-4001, USA*
[10]*Department of Physics, U.S. Naval Academy, Annapolis, Maryland 21402, USA*
[11]*Department of Chemistry and Biochemistry, University of Maryland, College Park, Maryland 20742, USA*
[12]*Hasan Ali Yucel Faculty of Education, Istanbul University, Beyazit, 34470 Istanbul, Turkey,*
[13]*National Institute for Physics and Nuclear Engineering, Bucharest-Magurele, Romania*

(Received 27 November 2006; published 18 October 2007)

High-spin states of ^{191,193}Au and ^{192}Pt have been populated in the ^{186}W(^{11}B, xn) and ^{186}W(^{11}B, p4n) reactions, respectively, at a beam energy of 68 MeV and their γ decay was studied using the YRAST Ball detector array at the Wright Nuclear Structure Laboratory at Yale University. The level scheme of ^{193}Au has been extended up to $I^{\pi} = 55/2^{+}$. New transitions were observed also in ^{191}Au and ^{192}Pt. Particle-plus-Triaxial-Rotor (PTR) and Total Routhian Surface (TRS) calculations were performed to determine the equilibrium deformations of the Au isotopes. The predictions for oblate deformations in these nuclei are in agreement with the experimental data. Development of nonaxial shapes is discussed within the framework of the PTR model.

DOI: 10.1103/PhysRevC.76.044315 PACS number(s): 29.30.Kv, 21.60.Ev, 23.20.Lv, 27.80.+w

I. INTRODUCTION

The $A \approx 190$ Au nuclei lie in a transitional region, where prolate-oblate shape change is expected to occur and the heavier isotopes are expected to take oblate shapes with moderate deformations, $\beta_2 \leqslant 0.15$ [1–3], while the lighter neutron-deficient nuclei are prolate rotors. Shape coexistence and shape changes in this region have been studied for decades and remain active topics in current research; e.g., a phase/shape transition has been suggested recently for the Pt isotopes [4] and the related critical point symmetries have been considered in this region [5,6]. It has been shown that the axially symmetric Particle-plus-Rotor (PR) model could not reproduce the properties of the low-lying oblate deformed states and it has been necessary to introduce γ deformation [7,8]. It has been demonstrated that nonaxiality in ^{191}Au is induced by the odd proton [9].

This article reports new experimental data in ^{191,193}Au and ^{192}Pt, e.g., in the case of ^{193}Au the level scheme is extended up to $I^{\pi} = 55/2^{+}$. This work (i) aims at detailed experimental study of the high-spin states in ^{193}Au and (ii) addresses the shape evolution for the Au isotopes.

The decoupled bands, which are known in the odd-mass Au isotopes, are built on $I^{\pi} = 11/2^{-}$ states, originating from the $\pi h_{11/2}$ subshell. For nuclei with oblate deformation the odd proton occupies a low-Ω $h_{11/2}$ orbital. There is a strong similarity between $\pi h_{11/2}$ bands in the odd-mass $^{185-195}$Au nuclei and ground-state bands in the Hg isotopes, which have been interpreted as a hole in the $\pi h_{11/2}$ subshell coupled to the corresponding Hg core [2,10,11]. This similarity holds also at higher spins [12].

Strongly coupled bands, which are built on the $9/2^{-}$ level, are known in these nuclei and are associated with the $\pi h_{9/2}$ configuration at oblate deformation [13]. In this work we have established the unfavored sequence of this band in ^{193}Au and have expanded it to higher spins in ^{191}Au. These new data allow a comparison with Particle-plus-Triaxial-Rotor model (PTR) calculations and a study of the equilibrium deformations in these nuclei.

The experimental procedure is described in Sec. II and the results are discussed in Sec. III. We note that these experimental results are presented in Ref. [14] and the results from PTR calculations are presented in Ref. [15].

II. EXPERIMENTAL PROCEDURE AND RESULTS

High-spin states of ^{193}Au were studied at the ESTU Tandem Van de Graaff accelerator at the Wright Nuclear Structure Laboratory of Yale University. The ^{186}W(^{11}B, 4n) fusion evaporation reaction at 68 MeV was utilized to populate high-spin states in ^{193}Au. The target consisted of three 300 μg/cm^2 ^{186}W foils. The cross section of the main 5n evaporation channel (^{192}Au) was calculated to be 570 mb, while the cross sections for the 4n (^{193}Au), 6n (^{191}Au), and p4n (^{192}Pt) channels were obtained as 20, 470, and 3.5 mb, respectively. Reaction γ rays

 ©2007 The American Physical Society

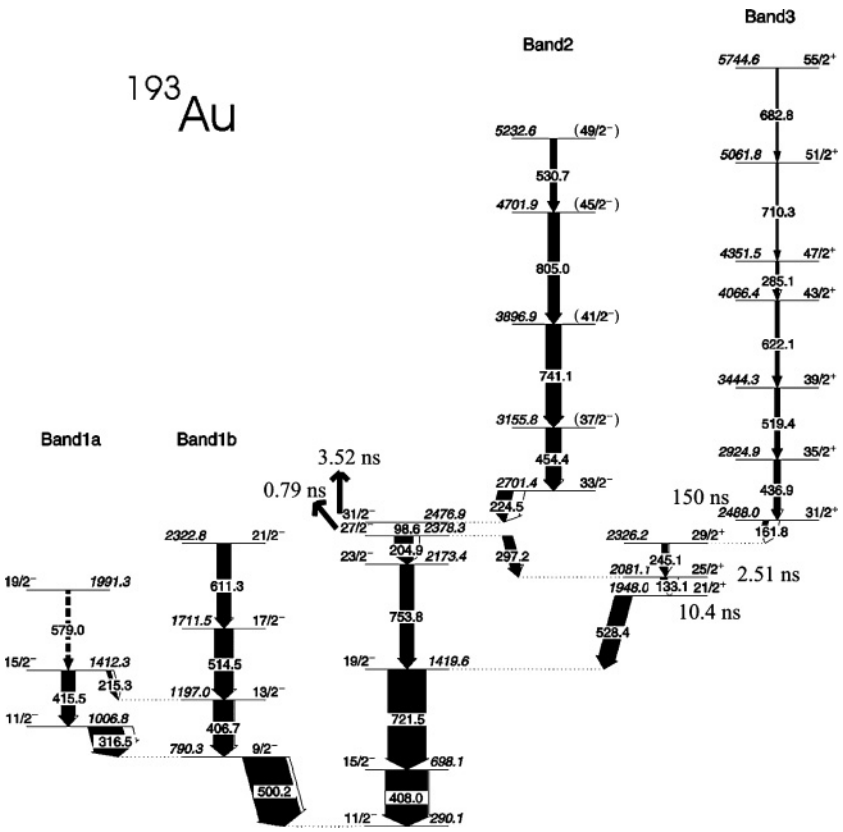

FIG. 1. Level scheme of ^{193}Au, as deduced from the ^{186}W(^{11}B, 4n) reaction at 68 MeV.

were detected in-beam with the YRAST Ball detector array [16], which consists of 7 Clover detectors, 16 single-crystal Ge detectors, and 3 LEPs detectors (to detect low energies) for this experiment. The trigger condition required at least three coincident γ rays to deposit their energy in a Clover or a single-crystal detector. Approximately 10^7 threefold and higher coincidence events were collected, which were sorted into a three-dimensional histogram using the Radware package [17].

The analysis of the data involved (i) study of the γ-ray coincidence relationships, (ii) angular distribution and linear polarization measurements to deduce the spin and parity of the levels, and (iii) γ-ray intensity measurements.

A. High-spin states in ^{193}Au

The level scheme of ^{193}Au, which has been deduced from these data, is presented in Fig. 1. All transitions that have been established for ^{193}Au are presented in Table I, together with the energies; the relative intensities; the DCO (directional correlations from oriented states) ratios, $R_{\rm DCO}$; the linear polarization ratios, $A_{\rm pol}$; and the deduced γ-ray multipolarity. The order of the γ rays is based on coincidence relationships and intensities. The multipolarity of γ rays has been determined from the experimental $R_{\rm DCO}$ and $A_{\rm pol}$ ratios. The $R_{\rm DCO}$ ratio provides information about the spin difference between the levels, while $A_{\rm pol}$ allows one to distinguish between γ rays of electric and magnetic type.

A two-dimensional angular correlation matrix was used to deduce the experimental $R_{\rm DCO}$ ratios. To construct this matrix, γ rays detected by a ring of seven Clover detectors at 90° with respect to the beam axis were sorted against the other three detectors at 160°. For the DCO analysis, most of the ratios were obtained when gating on the 408.0 keV stretched quadrupole $E2$ transition at the bottom of the level scheme in Fig. 1. If the gating transition is $E2$, the $R_{\rm DCO}$ ratios are approximately equal to 1.0 for $E2$ transitions, 0.5 for stretched $E1$ or $M1$ dipole transitions, and take intermediate values for mixed $M1/E2$ transitions. The ratios for the transitions on the left-hand side of the level scheme in Fig. 1 were deduced after gating on the 500.2 keV mixed $M1/E2$ transition. In this case, the $R_{\rm DCO}$ ratios are approximately equal to 1.1 for $E2$ transitions and take smaller values for mixed $M1/E2$ transitions, as seen from Table I.

The Clover detectors, which are positioned at 90° in YRAST Ball, were used as in-beam Compton polarimeters [18]. At this angle, the polarization is directly proportional to the experimental asymmetry, which is defined as $A_{\rm pol} = (N_\perp - N)/(N_\perp + N)$, where $N_\perp$ is the number of Clover add-back events that are due to Compton scattering at 90° with respect to the reaction plane and N is the number of events due to scattering parallel to the reaction plane. In Table I, positive values of the polarization parameter $A_{\rm pol}$ correspond to electric transitions, while negative values reveal magnetic transitions. All this information allowed us to fix the spin and parity of the levels in ^{193}Au. The γ-ray intensities have been normalized to the 500.2 keV $9/2^- \rightarrow 11/2^-$ transition. Sample spectra, revealing the transitions of the different sequences in ^{193}Au, are displayed in Fig. 2.

A decoupled sequence, built on the $11/2^-$ isomer ($T_{1/2} = 3.9(3)$ s), was known in ^{193}Au. The DCO and polarization measurements (see Table I) allow us to establish firmly the spins and parities in this band up to $27/2^-$. The spin and parity

TABLE I. The γ-ray energies, relative intensities, DCO ratios ($R_{\rm DCO}$), polarization ratios ($A_{\rm pol}$), and multipolarity assignments are shown for ^{193}Au as deduced from the ^{186}W(^{11}B, 4n) reaction at 68 MeV. The DCO and polarization ratios of some of the transitions could not be measured because of their weak intensities.

E_γ (keV)	E_i (keV)	$I_i^\pi \rightarrow I_f^\pi$	I ($\triangle I$)	$R_{\rm DCO}$ ($\triangle R_{\rm DCO}$)	$A_{\rm pol}$ ($\triangle A_{\rm pol}$)	Multipolarity
98.6 (1)	2476.9	$31/2^- \rightarrow 27/2^-$	18.6 (50)	–	–	–
133.1 (1)	2081.1	$25/2^+ \rightarrow 21/2^+$	48.7 (30)	1.2 (4)	–	$E2$
161.8 (1)	2488.0	$31/2^+ \rightarrow 29/2^+$	40.3 (24)	0.61 (9)	–	$M1$
204.9 (1)	2378.3	$27/2^- \rightarrow 23/2^-$	136.4 (16)	1.04 (9)	0.12 (7)	$E2$
215.3 (4)	1412.3	$15/2^- \rightarrow 13/2^-$	10.3 (56)	0.75 (13)	−0.07 (19)	$M1/E2$
224.5 (2)	2701.4	$33/2^- \rightarrow 31/2^-$	109.1 (17)	0.80 (9)	−0.05 (10)	$M1/E2$
245.1 (5)	2326.2	$29/2^+ \rightarrow 25/2^+$	47.3 (25)	1.01 (26)	0.10 (7)	$E2$
285.1 (7)	4351.5	$47/2^+ \rightarrow 43/2^+$	21.0 (61)	1.14 (19)	0.11 (11)	$E2$
297.2 (8)	2378.3	$27/2^- \rightarrow 25/2^+$	73.1 (16)	0.54 (9)	0.11 (12)	$E1$
316.5 (2)	1006.8	$11/2^- \rightarrow 9/2^-$	80.2 (11)	0.88 (12)	−0.09 (10)	$M1/E2$
406.7 (9)	1197.0	$13/2^- \rightarrow 9/2^-$	48.4 (15)	1.17 (29)	0.05 (13)	$E2$
408.0 (1)	698.1	$15/2^- \rightarrow 11/2^-$	307.0 (10)	–	–	$E2$
415.5 (9)	1412.3	$15/2^- \rightarrow 11/2^-$	33.0 (10)	1.23 (23)	0.04 (15)	$E2$
436.9 (1)	2924.9	$35/2^+ \rightarrow 31/2^+$	46.0 (28)	1.14 (18)	0.08 (13)	$E2$
454.4 (1)	3155.8	$37/2^- \rightarrow 33/2^-$	105.0 (16)	1.09 (22)	0.12 (13)	$E2$
500.2 (3)	790.3	$9/2^- \rightarrow 11/2^-$	100.0 (5)	–	–	$M1/E2$
514.5 (9)	1711.5	$17/2^- \rightarrow 13/2^-$	44.2 (57)	1.04 (24)	0.14 (13)	$E2$
519.4 (4)	3444.3	$39/2^+ \rightarrow 35/2^+$	36.1 (41)	1.06 (31)	0.08 (14)	$E2$
528.4 (4)	1948.0	$21/2^+ \rightarrow 19/2^-$	123.0 (24)	0.87 (13)	0.06 (11)	$E1$
530.7 (9)	5232.6	$49/2^- \rightarrow 45/2^-$	47.0 (39)	1.04 (23)	0.10 (10)	$E2$
579.0 (9)	1991.3	$19/2^- \rightarrow 15/2^-$	10.0 (12)	1.19 (33)	0.11 (9)	$E2$
611.3 (8)	2322.8	$21/2^- \rightarrow 17/2^-$	33.0 (12)	1.13 (32)	0.02 (19)	$E2$
622.1 (3)	4066.4	$43/2^+ \rightarrow 39/2^+$	29.6 (60)	1.08 (19)	0.11 (13)	$E2$
682.8 (9)	5744.6	$55/2^+ \rightarrow 51/2^+$	9.4 (82)	0.96 (21)	0.05 (14)	$E2$
710.3 (9)	5061.8	$51/2^+ \rightarrow 47/2^+$	10.3 (99)	1.03 (31)	0.12 (15)	$E2$
721.5 (3)	1419.6	$19/2^- \rightarrow 15/2^-$	279.0 (14)	1.07 (7)	0.06 (3)	$E2$
741.1 (4)	3896.9	$41/2^- \rightarrow 37/2^-$	107.0 (16)	1.07 (13)	0.13 (6)	$E2$
753.8 (5)	2173.4	$23/2^- \rightarrow 19/2^-$	99.3 (20)	1.17 (35)	0.08 (2)	$E2$
805.0 (1)	4701.9	$45/2^- \rightarrow 41/2^-$	81.3 (26)	0.94 (23)	0.04 (9)	$E2$

of the $I^\pi = 31/2^-$ isomer ($T_{1/2} = 3.52(18)$ ns [12]), which decays to the $I^\pi = 27/2^-$ level via the 98.6 keV transition, was accepted in accordance with the systematics of similar structures in the neighboring nuclei; e.g., in ^{191}Au the first $31/2^-$ state is a 6.1 ns isomer [9].

We confirm the transitions in Band 2, which were reported previously [13]. A sequence of stretched $E2$ transitions was suggested on top of the $31/2^-$ isomer. Spin and parity $I^\pi = (35/2^-)$ were tentatively assigned to the 2701.4 keV level [19] in Band 2. The measured DCO ratio $R_{\rm DCO} = 0.80(9)$ and the polarization coefficient $A_{\rm pol} = -0.05(10)$ for the 224.5 keV transition indicate that this is most likely a mixed $M1/E2$ transition; thus $I^\pi = 33/2^-$ was assigned to the 2701.4 keV level and negative parity was established for this sequence. Two new transitions were added on top of Band 2, which becomes a sequence of four stretched $E2$ transitions, built above the 2701.4 keV level, reaching spin $I^\pi = 49/2^-$. It should be noted, however, that a similar sequence above the $31/2^-$ isomer was observed in ^{191}Au (see sequence (b) in Fig. 1 of Ref. [9]). There, the most intensive transition on top of the isomer is the 301 keV dipole transition, in agreement with the present results for the 224.5 keV transition in ^{193}Au. On top of it, there is a 77 keV transition, which is strongly converted and has been established in an internal conversion experiment [9]. Parallel to these two transitions there is a stretched $E2$ transition, having roughly half of the intensity of the 301 keV transition. In ^{193}Au we observed only the 224.5 keV dipole transition to feed the $31/2^-$ state. This might be due to the low cross section of this reaction channel. Following the systematics argument, we cannot exclude the possibility that the observed cascade of Band 2 feeds the $35/2^-$ level and there exists a dipole transition with low energy that is not observed in our experiment.

A sequence of transitions, labeled as Band 1b, which is built on the $9/2^-$ level, was known in ^{193}Au [13]. This sequence decays to the $11/2^-$ state via a 500 keV transition. We observe a 407 keV $13/2^- \rightarrow 9/2^-$ transition (instead of the suggested 404 keV transition [19]) and unambiguously determine its $E2$ character. Two more stretched quadrupole transitions were observed in this band. Another sequence of levels, labeled as Band 1a, was found to decay to Band 1b via two interband transitions. The measured $R_{\rm DCO} = 0.88(12)$ and $A_{\rm pol} = -0.09(10)$ suggest that this is a mixed $M1/E2$ transition. Thus, spin-parity $I^\pi = 11/2^-$ is assigned to the 1007 keV level. Two transitions were observed in this sequence; the second of them is tentatively assigned.

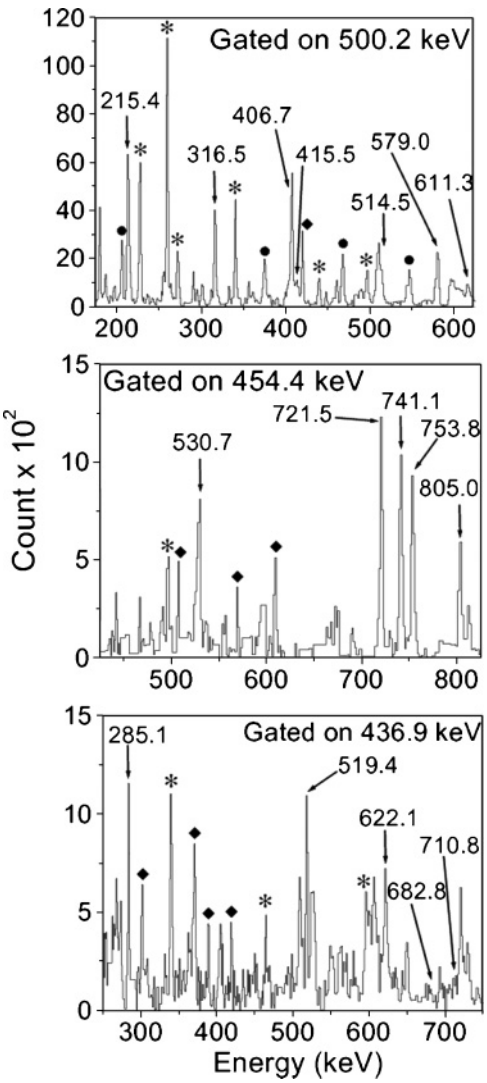

FIG. 2. Spectra showing single gates on the 500.2 keV, 454.4 keV, and 436.9 keV transitions, which reveal the γ-rays in ^{193}Au. Contaminating peaks labeled with $*$ belong to ^{192}Au, with ♦ belong to ^{191}Au, and with • belong to ^{192}Pt.

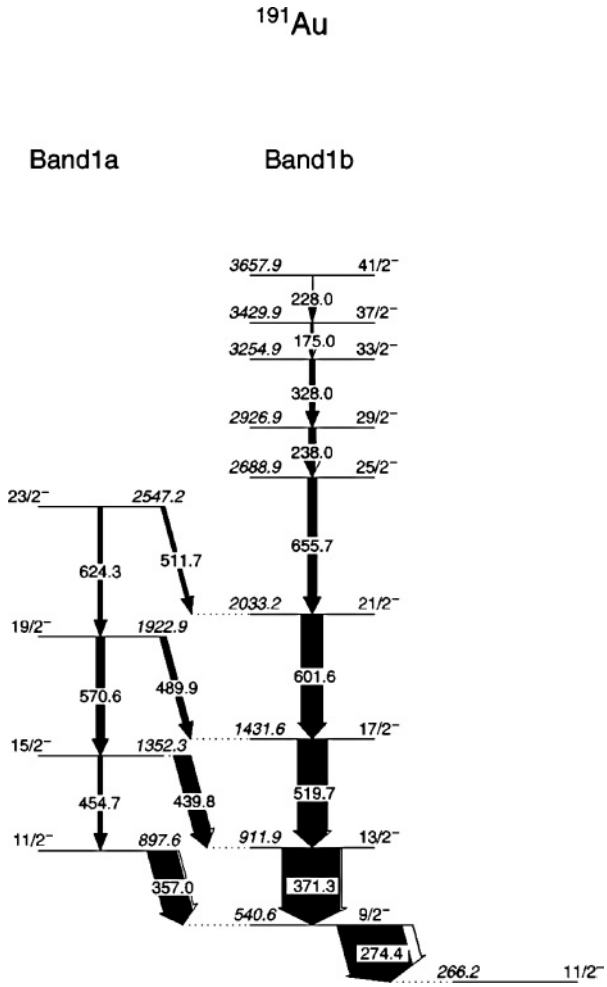

FIG. 3. Partial level scheme of ^{191}Au, as deduced from the ^{186}W(^{11}B, 6n) reaction at 68 MeV.

A sequence of three transitions, which is built on the $I^{\pi} = 31/2^{+}$ 150 ns isomer (denoted as Band 3), was known in ^{193}Au [13]. Three new transitions were added on the top of this sequence and it was extended up to $I^{\pi} = 55/2^{+}$. Band 3 is similar to the sequence, observed above the 402 ns isomer in ^{191}Au [9], except for the last transition of 710 keV.

B. Band structures in ^{191}Au

High-spin states in ^{191}Au have been studied recently and a detailed level scheme is presented in Ref. [9]. A band structure built on the $9/2^{-}$ state, which decays to the $11/2^{-}$ isomer ($T_{1/2} = 0.92(11)$ s), was found in ^{191}Au [20]. Three levels in a favored rotational aligned band (Band 1b in Fig. 3), and two levels in an unfavored band (Band 1a), were found [13]. Five transitions were added to Band 1b up to spin-parity $41/2^{-}$ [9]. In this experiment, we have established two new in-band transitions, belonging to the unfavored sequence and two new intraband transitions to Band 1b. A partial level scheme of ^{191}Au and sample spectra, showing the transitions in the favored and unfavored sequence of the $h_{9/2}$ band in ^{191}Au, are displayed in Fig. 3 and Fig. 4, respectively. Spectroscopic information about transitions, which belong to this sequence in ^{191}Au, is presented in Table II.

C. High-spin states in ^{192}Pt

Excited states in ^{192}Pt were weakly populated in this experiment. The ground-state band in this nucleus was known up to $I^{\pi} = 20^{+}$ [21]. A partial level scheme, as deduced from our data is presented in Fig. 5. Eleven new transitions were observed and ten new levels were added to the level scheme that belong to structures decaying to the yrast band in this nucleus. Spectroscopic information about the transitions in ^{192}Pt is presented in Table III. The DCO and polarization measurements support the spin-parity assignments in the ground-state band [21]. From the present data it is difficult to assign spin and parity to the new levels. Spins and parities in parentheses are estimated following the systematics in the region. Sample spectra, revealing some of the transitions in this nucleus, are presented in Fig. 6.

TABLE II. The γ-ray energies, relative intensities, DCO ratios (R_{DCO}), polarization ratios (A_{pol}), and multipolarity assignments are shown for ^{191}Au as deduced from the ^{186}W(^{11}B, 6n) reaction at 68 MeV. The DCO and polarization ratios of some of the transitions could not be measured because of their weak intensities.

E_γ (keV)	E_i (keV)	$I_i^\pi \rightarrow I_f^\pi$	I ($\triangle I$)	R_{DCO} ($\triangle R_{DCO}$)	A_{pol} ($\triangle A_{pol}$)	Multipolarity
175.0 (5)	3429.9	$37/2^- \rightarrow 33/2^-$	4.1 (1)	1.03 (3)	0.20 (15)	$E2$
228.0 (2)	3657.9	$41/2^- \rightarrow 37/2^-$	0.9 (1)	1.05 (2)	–	$E2$
238.0 (5)	2926.9	$29/2^- \rightarrow 25/2^-$	12.5 (4)	1.04 (3)	0.10 (15)	$E2$
274.4 (1)	540.6	$9/2^- \rightarrow 11/2^-$	100.0 (1)	–	–	$M1/E2$
328.0 (3)	3254.9	$33/2^- \rightarrow 29/2^-$	9.1 (3)	1.07 (4)	0.07 (11)	$E2$
357.0 (1)	897.6	$11/2^- \rightarrow 9/2^-$	44.0 (5)	0.73 (1)	−0.22 (1)	$M1/E2$
371.3 (1)	911.9	$13/2^- \rightarrow 9/2^-$	91.4 (9)	1.09 (1)	0.003 (10)	$E2$
439.8 (2)	1352.3	$15/2^- \rightarrow 13/2^-$	25.4 (4)	0.72 (2)	−0.13 (19)	$M1/E2$
454.7 (8)	1352.3	$15/2^- \rightarrow 11/2^-$	6.0 (2)	1.02 (3)	0.12 (10)	$E2$
489.9 (6)	1922.9	$19/2^- \rightarrow 17/2^-$	14.0 (3)	0.75 (3)	−0.21 (13)	$M1/E2$
511.7 (1)	2547.2	$23/2^- \rightarrow 21/2^-$	18.5 (4)	–	−0.07 (13)	$M1/E2$
519.7 (2)	1431.6	$17/2^- \rightarrow 13/2^-$	45.7 (6)	1.07 (2)	0.01 (9)	$E2$
570.6 (9)	1922.9	$19/2^- \rightarrow 15/2^-$	9.7 (3)	1.08 (3)	0.06 (1)	$E2$
601.6 (2)	2033.2	$21/2^- \rightarrow 17/2^-$	30.1 (7)	1.10 (2)	0.01 (14)	$E2$
624.3 (8)	2547.2	$23/2^- \rightarrow 19/2^-$	4.8 (2)	0.92 (4)	0.13 (16)	$E2$
655.7 (3)	2688.9	$25/2^- \rightarrow 21/2^-$	19.3 (4)	0.99 (3)	0.10 (17)	$E2$

III. DISCUSSION

The shape of the $A \approx 190$ Hg and Au nuclei changes from oblate for the $_{80}$Hg isotopes [22] to triaxial (induced by the odd proton in the $h_{11/2}$ orbital) [9,23] for the $_{79}$Au nuclei. TRS calculations [24] for the $N = 114$ isotones, ^{192}Pt and ^{193}Au, are displayed in Fig. 7. The odd proton is in the $h_{11/2}$ orbital for ^{193}Au. The potential energy surface for ^{192}Pt is very unstable with respect to γ deformation. A much better defined triaxial minimum with $\gamma \approx -75^\circ$ is predicted for ^{193}Au, and this nucleus keeps its triaxial shape beyond the first band crossing, as shown in the right-hand-side diagrams in Fig. 7. It should be noted that oblate shape is predicted to stabilize for ^{193}Au (at $\gamma \approx -77^\circ$) beyond the first band crossing, while, on the other hand, for ^{192}Pt the potential energy surface remains soft with respect to γ (see Fig. 7). The quadrupole deformation for ^{192}Pt, $\beta_2 \approx 0.15$, is slightly higher as compared to $\beta_2 \approx 0.13$ for ^{193}Au.

TABLE III. The γ-ray energies and relative intensities are shown for ^{192}Pt as deduced from the ^{186}W(^{11}B, p4n) reaction at 68 MeV.

E_γ (keV)	E_i (keV)	$I_i^\pi \rightarrow I_f^\pi$	I ($\triangle I$)
104.8 (2)	2623.7	$12^+ \rightarrow 10^+$	6.5 (13)
122.1 (2)	2641.0	$(12^+) \rightarrow 10^+$	5.0 (12)
147.0 (5)	2770.7	$(13^+) \rightarrow 12^+$	11.0 (12)
227.5 (3)	2998.2	$14^+ \rightarrow (13^+)$	10.0 (14)
274.0 (3)	3778.7	$(18^+) \rightarrow (16^+)$	6.3 (10)
316.5 (1)	316.5	$2^+ \rightarrow 0^+$	100.0 (1)
320.0 (2)	3504.7	$(16^+ \rightarrow (15^+)$	8.0 (21)
374.5 (5)	2998.2	$14^+ \rightarrow 12^+$	34.0 (30)
414.0 (5)	3184.7	$(15^+) \rightarrow (13^+)$	10.0 (21)
421.0 (3)	4199.7	$(20^+) \rightarrow (18^+)$	6.0 (11)
427.3 (1)	3068.3	$(14^+) \rightarrow (12^+)$	5.4 (13)
468.0 (4)	784.5	$4^+ \rightarrow 2^+$	GATE
489.4 (8)	3674.1	$(17^+) \rightarrow (15^+)$	9.2 (15)
500.6 (1)	2518.9	$10^+ \rightarrow 8^+$	54.0 (37)
505.0 (1)	2523.3	$(10^+) \rightarrow 8^+)$	11.0 (15)
543.9 (6)	3542.1	$16^+ \rightarrow 14^+$	12.1 (18)
580.9 (2)	1365.4	$6^+ \rightarrow 4^+$	94.4 (2)
614.0 (3)	3137.3	$12^+ \rightarrow 10^+$	7.4 (13)
652.9 (1)	2018.3	$8^+ \rightarrow 6^+$	60.0 (40)
662.1 (4)	4204.2	$18^+ \rightarrow 16^+$	14.1 (15)
746.5 (5)	4950.7	$(20^+) \rightarrow 18^+$	11.0 (14)

A. Band crossings in ^{193}Au

In ^{191,193}Au the $h_{11/2}$ band is terminated by the $27/2^-$ state, which is a $T_{1/2} = 0.79(8)$ ns isomer in ^{193}Au [12]. This state is understood as the coupling of a $\pi h_{11/2}$ hole either to the 8^+ state or to the 10^+ isomer in the core nucleus ^{194}Hg, which is considered to have three holes in the $\pi h_{11/2}$

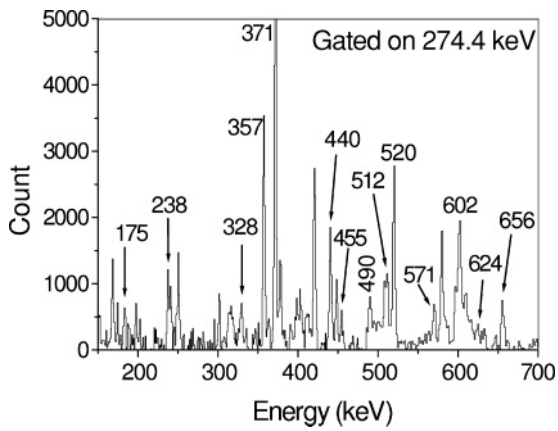

FIG. 4. Coincidence spectrum gated on the 274.4 keV transition for ^{191}Au.

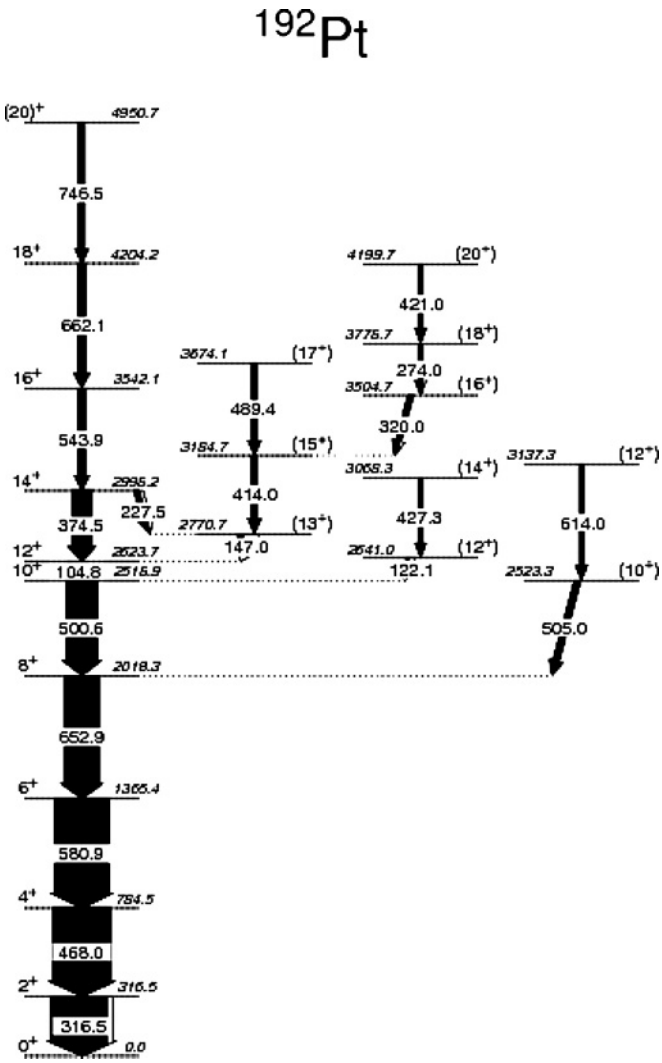

FIG. 5. Partial level scheme of ^{192}Pt, as deduced from the ^{186}W(^{11}B, p4n) reaction at 68 MeV.

orbit. The relatively low excitation energy of the $27/2^-$ state is understood to be due to the reduction of the pairing-gap energies in the odd-mass Au nuclei [25].

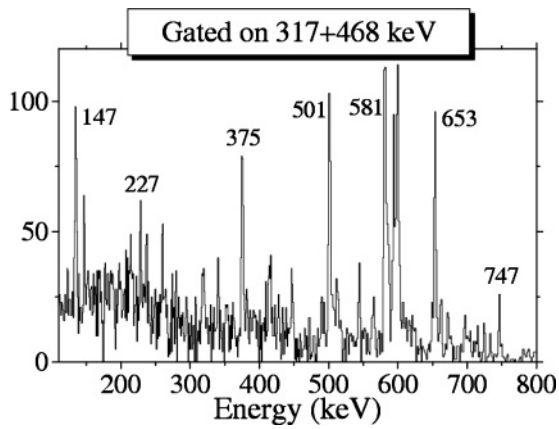

FIG. 6. Coincidence spectrum double gated on the 317 keV and 468 keV transitions, which reveals the γ rays in ^{192}Pt.

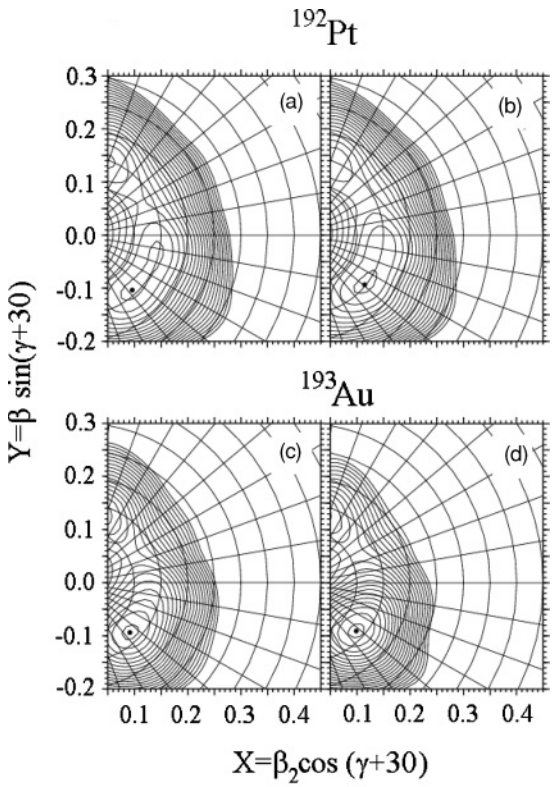

FIG. 7. (Top) TRS plots for ^{192}Pt calculated for (a) $\hbar\omega = 0.0$ MeV ($I = 0$), which displays a potential minimum for $\gamma = -77.2^\circ$, and (b) $\hbar\omega = 0.166$ MeV ($I = 14.3$), with a minimum for $\gamma = -69.2^\circ$. (Bottom) TRS plots for ^{193}Au calculated for (c) $\hbar\omega = 0.127$ MeV ($I = 6.2$), which displays a potential minimum for $\gamma = -75.8^\circ$, and (d) $\hbar\omega = 0.205$ MeV ($I = 18.8$), with a minimum for $\gamma = -72.6^\circ$.

The first band crossing in the $N = 114$ isotones is due to the alignment of a pair of $i_{13/2}$ neutrons [22]. The measured g factor of the $31/2^-$ isomer in ^{187}Au supports a $\pi h_{11/2}^{-1} i_{13/2}^{-2}$ configuration for this state [26]. We suggest that the $31/2^-$ state in ^{193}Au has the same configuration.

Alignment plots and experimental Routhians for the ground-state bands in ^{192}Pt and ^{194}Hg and for the $\pi h_{11/2}$ band in ^{193}Au are displayed in Fig. 8. For an easier comparison, the alignment curves for ^{193}Au are shifted down by $5.5\hbar$, which is the initial alignment of the $h_{11/2}$ proton (the proper values for this band can be seen on the right-hand-side scale in Fig. 8). The reference parameters are $J_0 = 10\hbar^2\,\mathrm{MeV}^{-1}$ and $J_1 = 55\hbar^4\,\mathrm{MeV}^{-3}$ for ^{192}Pt [27], $J_0 = 6\hbar^2\,\mathrm{MeV}^{-1}$ and $J_1 = 30\hbar^4\,\mathrm{MeV}^{-3}$ for ^{193}Au [9], and $J_0 = 8\hbar^2\,\mathrm{MeV}^{-1}$ and $J_1 = 40\hbar^4\,\mathrm{MeV}^{-3}$ for ^{194}Hg [22]. A backbending with an alignment gain of $\Delta i \approx 12\hbar$ occurs in all three nuclei at a rotational frequency $\hbar\omega_c \approx 0.22$ MeV, in perfect agreement with the TRS calculations, where an alignment gain of $12\hbar$ is obtained for a rotational frequency $\hbar\omega_c \approx 0.20$ MeV, as indicated in the figure legend of Fig. 8. If we accept that Band 2 in ^{193}Au is built on the $35/2^-$ state, the alignment gain would be $1\hbar$ larger and consistent with those in other $N = 114$ isotones (not indicated on the figure).

New transitions, which were established to belong to Band 2 in ^{193}Au, witness that a second bandcrossing occurs in this

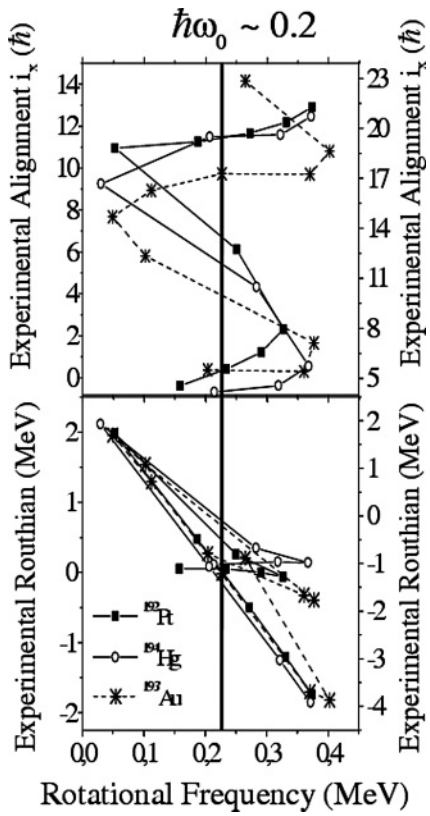

FIG. 8. The experimental alignments (top) and Routhians (bottom) for the ground-state bands in ^{192}Pt and ^{194}Hg and the $\pi h_{11/2}$ band in ^{193}Au. The alignment for ^{193}Au has been reduced by $11/2\hbar$ to simplify comparison with the data from the neighboring nuclides.

sequence. A second pair of $i_{13/2}$ neutrons is expected to align above spin $47/2^-$, in agreement with the systematic trends in the lighter odd-A Au nuclei and their Hg isotones. A similar band crossing has been observed in ^{191}Au [9], which has been interpreted as a second $\nu i_{13/2}$ crossing.

The $21/2^+$ states in the odd-mass Au nuclei are observed at excitation energies comparable to those of the $5^-\nu(p_{3/2}i_{13/2})_{5^-}$ states in the Hg nuclei and are interpreted as due to the coupling of a $\pi h_{11/2}$ to the 5^- states in the Hg isotopes [11]. Similarly, the $25/2^+$ states result from coupling of $h_{11/2}$ protons to 7^- states in the Hg nuclei [13].

The $31/2^+$ state in ^{193}Au is a long-lived positive parity isomer with a half-life of 150 ns [12]. Isomeric levels with $I^\pi = 31/2^+$ are known in the odd-A Au nuclei and are associated with the $\pi h_{11/2} \otimes \nu(i_{13/2}h_{9/2})_{10^-}$ configuration [1,2,28,29], i.e., the $h_{11/2}$ protons couple to the $10^-\nu(i_{13/2}h_{9/2})_{10^-}$ states in the Pt nuclei. In ^{191}Au the same configuration has been proven for this state after a g-factor measurement [26]. A sequence of transitions (Band 3), which is built on this isomer, has been established in ^{193}Au. The band crossing observed above the $43/2^+$ level is due to the alignment of a pair of $i_{13/2}$ neutrons.

B. PTR calculations

To study the deformation of odd-A $^{187-193}$Au nuclei for the $\pi h_{9/2}$ configuration, PTR [30] calculations have been performed. Previously different attempts have been made to determine the equilibrium deformations of these nuclei with respect to the asymmetry parameter γ [31–36]. The results of these calculations are summarized in Table IV. In general, these calculations indicate that quadrupole deformation, β_2, decreases with an increase of the neutron number, while the triaxiality parameter γ increases.

TABLE IV. Equilibrium shape parameters β_2 and γ for the odd-mass Au nuclei, as deduced by different authors within the framework of the triaxial particle-plus-rotor model. HO denotes modified Harmonic Oscillator potential and WS stands for Woods-Saxon potential.

Nucleus	β_2	γ	Model	Reference
^{185}Au	+0.25	≈20°	HO	[31]
^{185}Au	+0.25	0°	PTR + HO	[32]
^{185}Au	+0.25	20°	PTR + WS	[33]
^{187}Au	+0.21	20°	PTR + WS	[34]
^{187}Au	+0.20	20°	PTR + HO	[32]
^{189}Au	–	23°	PTR	[36]
^{193}Au	+0.15	35°	PTR + HO	[32]
^{195}Au	+0.15	35°	PTR + HO	[32]

The new levels in the $h_{9/2}$ bands, reported here for ^{191,193}Au, allow a better comparison between experiment and PTR calculations. Experimental data for the $\pi h_{9/2}$ bands in $^{187-193}$Au are presented in Fig. 9. The data for ^{187}Au are from Ref. [2], and for ^{189}Au from Ref. [29]. This structure, which is built on the $1/2^-[541]$ Nilsson model state, appears as a decoupled band in the Au nuclei. In ^{187}Au $I+1$ levels of the unfavored sequence lie higher than the $I+2$ levels of the favored sequence. In ^{189,191}Au they are almost degenerate, while for ^{193}Au the $I+1$ levels are lower than the $I+2$ levels of the favored sequence. The transition takes place between ^{189}Au and ^{191}Au. Already Gono *et al.* [13] noticed this feature for the 11^- level and commented that it might be due to a transition from $\gamma < 30°$ (for ^{187}Au) to $\gamma > 30°$ (for ^{193}Au).

The numerical calculations were done with the GAMPN/ASYRMO code, using the modified oscillator potential, as described in Ref. [37]. The calculations yield the excitation energies of the levels in the band. The results of the calculations are presented on the left-hand side of Fig. 9 and in Table V.

Within the PTR model, we find a solution for these bands for which the triaxiality parameter varies from $\gamma = 12°$ for ^{187}Au, reaching oblate shape for ^{193}Au ($\gamma = 58°$). The quadrupole

TABLE V. Equilibrium shape parameters β_2 and γ for the odd-mass Au nuclei, as deduced within the framework of the triaxial particle-plus-rotor model with a modified harmonic oscillator potential.

Nucleus	β_2	γ
^{187}Au	+0.20(2)	12(2)°
^{189}Au	+0.22(2)	30(2)°
^{191}Au	+0.20(2)	43(2)°
^{193}Au	+0.18(2)	58(2)°

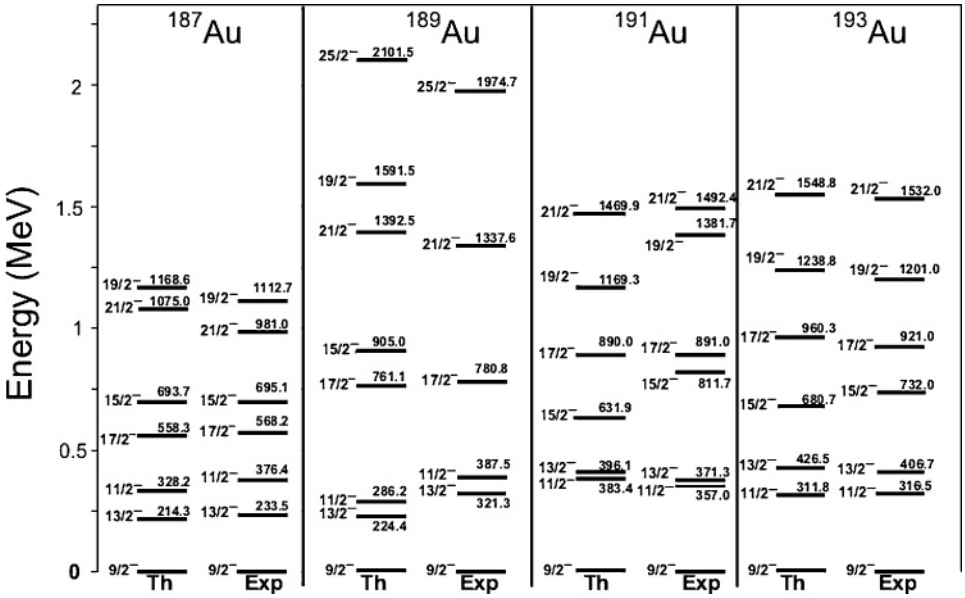

FIG. 9. Experimental levels in the $\pi h_{9/2}$ bands in the odd-mass ^{187,189,191,193}Au, compared to PTR calculations.

deformation takes values close to $\beta_2 = 0.2$ and there is a trend of a slight decrease with an increase of the neutron number. For ^{187}Au and ^{193}Au we obtain reasonable agreement between the calculated spectra and experiment, while for ^{189,191}Au the agreement is not very good. In the case of ^{189}Au this poor accuracy might be due to the fact that only five levels are known experimentally. The calculation for ^{191}Au above the $13/2^-$ level does not reproduce well the experimental spectrum, but the near-degeneracy of the $11/2^-$ and $13/2^-$ is obtained about right and the calculation yields the proper order of the levels above the $11/2^-$ state. We should note that the shape parameters listed in Table V should be considered as tentative. The important point is that they demonstrate a trend of prolate-to-oblate shape change. Berg *et al*. [32] have done PTR calculations (see Table IV). The deformation parameters that they obtain for ^{187}Au are rather similar to those from this work, while for ^{193}Au they differ considerably. The reason for it might be that in this work we have established a few more levels in this sequence, which are used in the fit and set more constrains to the calculation. The results of calculations have poor accuracy for ^{189}Au, which may be due to the fact that only five levels are known experimentally. It should be noted that a second solution exists for $\gamma \sim 0^\circ$ in reasonable agreement with the experiment [15]. In this case, the triaxiality parameter γ changes sign between ^{189}Au and ^{191}Au, but stays close to zero. However, we consider the former solution to be more likely because it corresponds to triaxial shapes which are expected to occur in these nuclei and are predicted also by other models. It is necessary to compare transition strengths to model predictions to provide a definite answer as to what are the equilibrium deformations for the Au nuclei in the $\pi h_{9/2}$ configuration. At present, data are lacking in all these cases: thus, this might be a motivation for future experimental studies.

IV. CONCLUSIONS

In summary, the level scheme of ^{193}Au was extended significantly. New levels were established also in ^{191}Au and ^{192}Pt. Two band crossings were established for the $h_{11/2}$ band in ^{193}Au, which are due to the alignment of two pairs of $i_{13/2}$ neutrons with an oblate shape. PTR model calculations were performed that demonstrate that the quadrupole deformation decreases with increasing neutron number for the odd-mass $^{187-193}$Au nuclei in the $h_{9/2}$ configuration, while the triaxiality parameter changes from $\gamma \approx 12^\circ$ to $\gamma \approx 58^\circ$, indicating that a prolate-to-oblate shape transition takes place in this region.

ACKNOWLEDGMENTS

The Sofia and Istanbul groups thank WNSL for the excellent working conditions. This work is supported by the U.S. DOE under Grants DE-FG02-91ER-40609 and DE-FG05-96ER40983, the Research Fund of Istanbul University under Projects 1582/19032001 and UDP-165/25062003, and the Bulgarian Science Fund under Project VUF06/05.

[1] C. Bourgeous *et al*., Z. Phys. A **333**, 5 (1989).
[2] J. K. Johansson *et al*., Phys. Rev. C **40**, 132 (1989).
[3] N. Perrin *et al*., Z. Phys. A **347**, 81 (1993).
[4] J. Jolie and A. Linnemann, Phys. Rev. C **68**, 031301(R) (2003).
[5] E. A. McCutchan, R. F. Casten, and N. V. Zamfir, Phys. Rev. C **71**, 061301(R) (2005).
[6] D. Bonatsos *et al*., Phys. Lett. **B588**, 172 (2004).
[7] Ch. Vieu *et al*., J. Phys. G **4**, 531 (1977); **4**, 1159 (1978).
[8] M. G. Porquet *et al*., Nucl. Phys. **A451**, 365 (1986).
[9] E. Gueorguieva *et al*., Phys. Rev. C **68**, 054308 (2003).
[10] M. A. Delepianque *et al*., Nucl. Phys. **A249**, 366 (1975).
[11] P. O. Tjom *et al*., Nucl. Phys. **A231**, 397 (1974).
[12] V. Kölscbach *et al*., Nucl. Phys. **A439**, 189 (1985).
[13] Y. Gono *et al*., Nucl. Phys. **A327**, 269 (1979).

[14] Y. Oktem, M.S. thesis, University of Istanbul, 2002, and Ph.D. thesis, University of Istanbul, 2005.
[15] N. I. Nikolov *et al*., in *Proceedings of the* 4th *Balkan School on Nuclear Physics, Bodrum, 2004,* Balkan Phys. Lett. Special Issue (2004), ISSN 1301-8329, p. 291.
[16] C. W. Beausang *et al*., Nucl. Instrum. Methods A **452**, 431 (2000).
[17] D. C. Radford, Nucl. Instrum. Methods Phys. Res. A **361**, 297 (1995).
[18] G. Duchene *et al*., Nucl. Instrum. Methods A **432**, 90 (1999).
[19] E. Achterberg, G. V. Marti, V. R. Vanin *et al*., Nucl. Data Sheets **107**, 1 (2006).
[20] H. Beuscher, P. Jahn, R. M. Lieder, and C. Mayer-Böricke, Z. Phys. **247**, 383 (1971).
[21] J. C. Cunnane *et al*., Phys. Rev. C **13**, 2197 (1976).
[22] H. Hubel *et al*., Nucl. Phys. **A453**, 316 (1986).
[23] E. Gueorguieva *et al*., Phys. Rev. C **69**, 044320 (2004).
[24] R. Wyss *et al*., Nucl. Phys. **A511**, 324 (1987).
[25] Y. Gono *et al*., Phys. Rev. Lett. **37**, 1123 (1976).
[26] N. Perrin *et al*., Z. Phys. A **359**, 373 (1997).
[27] T. Kutsarova *et al*., Eur. Phys. J. A **23**, 69 (2005).
[28] C. Bourgeous *et al*., Z. Phys. A **343**, 243 (1992).
[29] Ts. Venkova *et al*., Z. Phys. A **344**, 231 (1992).
[30] J. Meyer-ter-Vehn *et al*., Nucl. Phys. **A249**, 111 (1975).
[31] G. Passler *et al*., Nucl. Phys. **A580**, 173 (1994).
[32] V. Berg *et al*., Nucl. Phys. **A410**, 445 (1983).
[33] C. Ekström *et al*., Nucl. Phys. **A348**, 25 (1980).
[34] D. Rupnik, E. F. Zganjar, S. L. Wood, P. B. Semmes, and W. Nazarewicz, Phys. Rev. C **51**, 2867 (1995).
[35] D. Rupnik, E. F. Zganjar, S. L. Wood, P. B. Semmes, and P. F. Mantica, Phys. Rev. C **58**, 771 (1998).
[36] J. L. Wood *et al*., Phys. Rev. C **14**, 682 (1976).
[37] I. Ragnarsson and P. B. Semmes, Hyperfine Interact. **43**, 425 (1988).